Energy Conversion and Management 205 (2020) 112395

Contents lists available at ScienceDirect

Energy Conversion and Management

journal homepage: www.elsevier.com/locate/enconman

Research on the performance of radiative cooling and solar heating coupling module to direct control indoor temperature

Junwei Liu[a], Zhihua Zhou[a,*], Debao Zhang[a], Shifei Jiao[a], Ji Zhang[a], Feng Gao[b], Jihong Ling[a,*], Wei Feng[c], Jian Zuo[d]

[a] Tianjin Key Laboratory of Indoor Air Environmental Quality Control, Key Laboratory of Efficient Utilization of Low and Medium Grade Energy, School of Environmental Science and Engineering, Tianjin University, Tianjin, China
[b] School of Architecture, Tianjin University, Tianjin, China
[c] Lawrence Berkeley National Laboratory, Berkeley, CA, USA
[d] School of Architecture & Built Environment, The University of Adelaide, Adelaide 5005, Australia

ARTICLE INFO

Keywords:
Direct radiative cooling
Solar heating
Temperature-regulating module
Energy-saving
Economic analysis

ABSTRACT

The energy crisis and environmental pollution pose great challenges to human development. Traditional vapor-compression cooling consumes abundant energy and leads to a series of environmental problems. Radiative cooling without energy consumption and environmental pollution holds great promise as the next generation cooling technology, applied in buildings mostly in indirect way. In this work, a temperature-regulating module was introduced for direct summer cooling and winter heating. Firstly, the summer experiments were conduct to investigate the radiative cooling performance of the module. And the results indicated that the maximum indoor temperature reached only 27.5 °C with the ambient temperature of 34 °C in low latitude areas and the air conditioning system was on for only about a quarter of the day. Subsequently, the winter experiments were performed to explore the performance of the module in cooling and heating modes. The results indicated that indoor temperature can reach 25 °C in the daytime without additional heat supply and about a quarter of the day didn't require heating in winter. Additionally, the transient model of the module and the building revealed that the electricity saving of 42.4% (963.5 kWh) can be achieved in cooling season with the module, and that was 63.7% (1449.1 kWh) when coupling with energy storage system. Lastly, further discussion about the challenges and feasible solutions for radiative cooling to directly combine with the buildings were provided to advance the application of radiative cooling. Furthermore, with an acceptable payback period of 8 years, the maximum acceptable incremental cost reached 26.2 $/m^2. The work opens up a new avenue for the application mode of the daytime radiative cooling technology.

1. Introduction

Global warming has caused the rapid growth of hot days and extreme weather, extremely increasing the cooling demand. The widely used vapor-compression cooling not only consumes abundant energy, but also degrades the atmospheric ozone, leading to a series of environmental problems [1]. Generally, it is essential for the complex vapor-compression cooling systems to be equipped with cooling devices, rising the cooling cost and consuming extensive water (e.g. cooling towers, etc.) [2]. Passive radiative cooling without any energy input is a promising alternative to address the problems.

Radiative cooling dissipates the object's heat through the atmospheric window (8–13μm) to the ultra-cold outer space [3]. This cooling mechanism has been greatly investigated to achieve sub-ambient cooling at night [4]. However, the cooling peak occurs in the daytime, when the solar irradiation is high (~1000 W/m^2) [5], and the radiative cooling power is relatively low (~100 W/m^2) [6]. Therefore, the radiative coolers with low solar absorption are essential to achieve daytime radiative cooling [7]. In 2014, the pioneering work carried out by Stanford's Fan et al. [8] successfully broke through the daytime and nighttime restrictions of radiative cooling technology. They proposed a multilayer photonic radiative cooler, consisting of seven dielectric layers deposited on top of a silver coating. The maximum temperature drop (MTD) of 4.9 °C and a radiative cooling power at ambient temperature (RCPAT) of 40.1 W/m^2 were successfully achieved under the solar irradiation of 850 W/m^2. In 2015, Gentle et al. [9] employed

* Corresponding authors.
E-mail addresses: zhuazhou@tju.edu.cn (Z. Zhou), jihongling@tju.edu.cn (J. Ling).

https://doi.org/10.1016/j.enconman.2019.112395
Received 10 October 2019; Received in revised form 6 December 2019; Accepted 8 December 2019

Nomenclature

TRM	temperature-regulating module
SBED	the simulated building experimental device
SBCD	the simulated building control device
RCED	the general radiative cooling experimental device
$P_{rad}(t)$	instantaneous radiation intensity, W/m^2
$P_{sun}(t)$	instantaneous solar absorption intensity, W/m^2
$P_{cond+conv}(t)$	instantaneous non-radiative heat exchange intensity, W/m^2
$P_a(t)$	the load caused by temperature difference, W/m^2
$P_b(t)$	the load from sunlight absorbed by enclosure, W/m^2
$P_c(t)$	the load caused by sunlight entering the room through windows, W/m^2
$P_d(t)$	the load caused by human body, lighting and equipment, W/m^2
m	the air weight inside the building, kg
c_v	the constant volume heat capacity, J/(kg·K)
T	the inner air temperature, K
t	the calculating time, S
T_r	the function of the TRM temperature, K
$T_{dewpoint}$	the ambient dew point temperature, K
α_r	the solar absorption of cooling and heating mode
I_{sun}	the sunlight intensity s, W/m^2
A	the TRM area, m^2
T_{amb}	the ambient temperature, K
h_c	the non-radiative heat exchange coefficient, W/(m^2.K)
U_i	heat exchange coefficient of wall, window and roof respectively, W/(m^2.K)
A_i	area of wall, window and roof respectively, m^2
α_l	the solar absorptivity of each side of the enclosure
A_l	the area of each side of the enclosure, m^2
I_l	the incident intensity of sunlight on each side of the enclosure, W/m^2
τ	the solar transmittance of the window
A_t	the area of each window, m^2
I_t	the incident intensity of sunlight for each window, W/m^2
W	the load from human body, lighting and equipment per unit area, W/m^2
A_0	the building area, m^2
SPP	simple payback period, year
C_R	the cost of the building employing the TRM, $
C_A	the cost of the air conditioning system after employing the TRM, $
C_S	the cost of air conditioning, $
E_{S1}	the summer electricity consumption of the split air conditioning, kWh
E_{S2}	the winter electricity consumption of the split air conditioning, kWh
E_{A1}	the summer electricity consumption by employing the TRM and the split air conditioning, kWh
E_{A2}	the winter electricity consumption by employing the TRM and the split air conditioning, kWh
P_E	the electricity price, $/kWh
AIC_{max}	the maximum acceptable incremental cost, $/m^2

commercially available ESR film, which had high mid-infrared emissivity and can reflect part of the sunlight. The film with silver coating had a solar reflectivity of 97% and mid-infrared emissivity of 96% in the atmospheric window, indicating a great daytime cooling performance. In 2017, Kou et al. [10] employed fused quartz with high infrared emissivity and polydimethylsiloxane (PDMS) with the thickness of 100μm to improve the fused quartz emissivity. They achieved a MTD of 8.2 °C and a RCPAT of about 127 W/m^2 under direct solar radiation, higher than all the radiative cooling materials existing.

Additionally, to achieve the large-scale application, it is essential to develop simple and cost-effective the manufacturing technologies of the radiative cooling materials. In 2017, Zhai et al. [11] proposed a metamaterial consisting of a random embedded resonant polar dielectric microsphere SiO_2 into the polymer. And a solar reflectivity of 97% and mid-infrared emissivity of 93% in the atmospheric window were achieved. The metamaterial achieved an average daytime RCPAT of 93 W/m^2, when exposed to direct sunlight. In 2018, Atiganyanun et al. [12] optimized the size and filling rate of SiO_2 particles to minimize the average free path of solar light scattering, effectively reducing the sunlight absorption and enhancing the mid-infrared emissivity. The optimized cooling coating achieved a mid-infrared emissivity of 94% in the atmospheric window, and a MTD of 12 °C under direct solar radiation. Mandal et al. [13] employed the phase conversion method to optimize the intrinsic high infrared emission polymer to form the hierarchical porous cooling material, which can scatter visible and near infrared light, respectively and enhance the mid-infrared emissivity at the same time. The silver-free hierarchical porous cooling material achieved a solar reflectivity of 96% and an infrared emissivity of 97% in the atmospheric window. Additionally, a MTD of 6 °C and a daytime RCPAT of 96 W/m^2 were achieved w under the direct sunlight of 890 W/m^2. However, all these work was conducted to cool small thermal mass in a clear and cloudless day, yet the goal of actual application of radiative cooling technology was to cool large thermal mass (e.g. buildings, etc.) in various climates.

Radiative cooling applied in buildings mainly employed the indirect way, coupling with coils into the cooling module, which can reduce the energy consumption of the air conditioning system (mainly the condenser) by cooling the flowing working fluid. The modeling results indicated that the energy savings in cooling season can reach 21% [14] and 32%-45% (combined with energy storage system) [15], respectively. It was flexible to control the cooling input in indirect way, but it reversely meant that as long as the building need cooling, the air conditioning system must be on (or partially on), that is, the indirect way consumed abundant energy during the operation. Additionally, for superior heat exchange, the flow speed of working fluid in the cooling module was fairly slow (~0.29 L/ (h·m^2)) [16]. Whether the module was directly or indirectly coupled with the air conditioning system (through plate heat exchanger), it's laborious to achieve the great cooling performance in the actual system. Note that in some areas where the cooling load wasn't too huge in summer, radiative cooling can sufficiently meet the indoor cooling demand, while the indirect way will lead to extra energy consumption.

The direct combination of the nighttime radiative cooling technology and buildings (the direct way) was investigated in the past, but for daytime radiative cooling, the direct way was still unexplored. Radiative cooling was independent on the air conditioning system in direct way, indicating that when the cooling load was low, cooling modules worked alone and when the cooling load was large, cooling modules and air conditioning system jointly provided cooling. It was significantly promising to explore the direct way, due to the great energy saving potential and the extremely low initial investment.

For the low latitude areas with abundant cooling load, the direct way exerts a significant role in reducing the energy consumption. For mid-latitudes, it can meet or partly meet the cooling demand in summer, while the temperature in the transition season or winter will be exceedingly low in direct way, not only affecting the indoor comfort, but also rising the heating energy consumption (negative impact) [17]. Recent works have revealed that the thermosensitive phase change materials (VO_2 [18], $La_{0.7}Ca_{0.3-x}Sr_xMnO_3$ [19]) can effectively control the radiative cooling power, enhancing the mid-infrared emission of

radiative coolers at high temperature, and reducing mid-infrared emission at low temperature. However, the tunability and applicability of this material were limited, especially with a poor effect in winter.

In light of the negative impact of the direct way, a temperature-regulating module (TRM) based on the combination of radiative cooling and solar heating was proposed. In principle, radiative cooling can directly reduce the indoor temperature in summer, and the solar heating can be employed to raise the indoor temperature in winter. In the transitional season, it was flexible to control cooling or heating according to the actual need. To this end, the simulated building experimental device (SBED) with the TRM at top was manufactured and the summer and winter experiments were conducted in Sanya and Tianjin, respectively. Subsequently, energy saving of the single-storey residential building in mid-latitudes with or without energy storage system was modeled to explore the potential of the proposed module. Additionally, the economic analysis of the proposed module was investigated to further demonstrate the superiority of the direct combination of radiative cooling technology and buildings.

2. Experimental design

To investigate the direct combination of radiative cooling technology and buildings, a temperature-regulating module, cooling in summer and heating in winter, was firstly proposed. Additionally, cooling and heating experiments were designed to demonstrate the energy-saving potential of the TRM.

2.1. Temperature-regulating module

In view of the negative impact of radiative cooling in winter, a temperature-regulating module was proposed (Fig. 1a and b), consisted of a 10μm polyethylene film, a porous cooling material, an aluminum conductor and a solar absorbing material. Note that the porous cooling material not only has near-unity infrared emissivity in the atmospheric window, but also can effectively scatter sunlight through the hierarchically porous structure [13]. And the cost of this cooling material is rather low without employing the costly silver or other metals. Additionally, the solar absorbing material was coated with commercialized chromium plating, which has more than 95% solar absorptivity and low mid-infrared emissivity. The aluminum conductor supported the whole TRM to provide the essential strength, simultaneously providing good heat conduction. To maximize the potential of radiative cooling, it was significant to keep apart the cooling material from the surroundings. 10μm polyethylene film with high solar and infrared transmission was employed to reduce the non-radiative heat exchange between the cooling material and the surroundings.

There existed two operation modes of the TRM: cooling mode and heating mode. In cooling mode, solar radiation passed through thin polyethylene film and entered porous cooling material. After effectively scattering by the hierarchically porous structure, only extremely few solar radiation was absorbed by the TRM. Meanwhile, indoor heat was transferred to the TRM through convection and conduction. Finally, the heat was dissipated into outer space through the atmospheric window (Fig. 1a). In heating mode, most of the solar radiation was absorbed when entering the solar absorbing material. Subsequently, part of heat

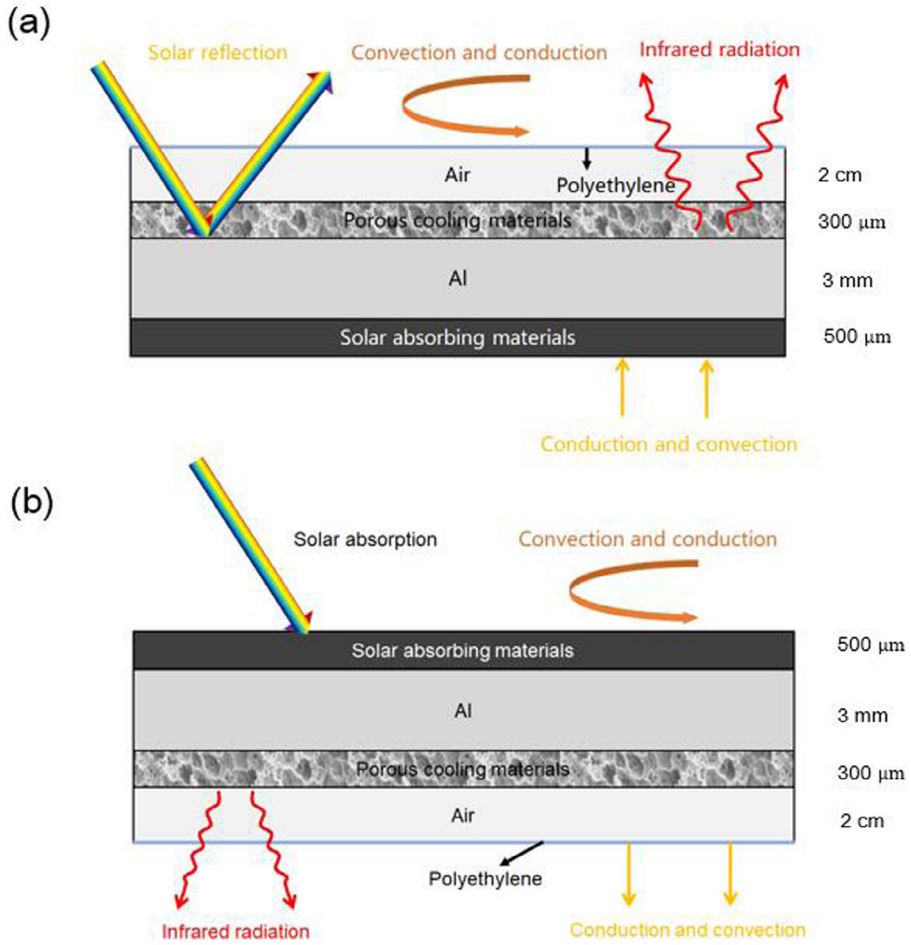

Fig. 1. The temperature-regulating module. (a) Schematics of temperature-regulating module in cooling mode. (b) Schematics of temperature-regulating module in heating mode (The thickness of each layer was provided on the right side of the module).

was transferred to the indoor through the thermal radiation, while the other part was exchanged to the indoor through convection and conduction (Fig. 1b).

2.2. Experimental device fabrication and measurement

The experimental devices were set up in Fig. 2a and b, including the simulated building experimental device (SBED), the simulated building control device (SBCD) and the general radiative cooling experimental device with thick insulation (RCED). The TRM with an area of 0.15 m^2 was employed as the SBED roof. And the sidewall and the bottom were made of polystyrene insulation material to mimic the building insulation with the outer surface wrapped with highly reflective foil to reduce the solar absorption. A graphene heater with a rated power of 0.5 W was introduced in inner space to mimic the cooling load caused by heat dissipation of human body, lighting and equipment. For consistency, the settings of SBCD were same as the SBED except for the TRM rooftop.

The SBED was well sealed into a 0.5 m× 0.3 m× 0.3m space (Fig. 2b and Fig. 3b), with the rooftop employing the 0.3 m×0.5 m TRM the side wall employing 0.01 m polymethyl methacrylate (PMMA) sheet and 0.04 m polystyrene insulation and the bottom employing 0.1 m polystyrene insulation. Note that the PMMA sheet was employed to support interior space and the polystyrene material was used to reduce heat exchange coefficient. This work employed the commercially available PMMA sheet with the thickness of 0.01 m. And the thickness of polystyrene insulation was determined via the heat flow and temperature tester, that is, the heat exchange coefficients of the PMMA and polystyrene binding layer should be less than 1 W/(m^2·K) to effectively reduce the heat exchange. There were three temperature measuring points placed at the top of the device, a temperature measuring point for each sidewall and three equal-distance temperature measuring points of inner air (Fig. 2b). The curves in the figures were the average value of corresponding measurement points. In heating experiment, an electric heater was essential to mimic building heating supply in the winter of mid-latitudes. The heater with rated voltage of 220 V and rated power of 25 W was employed to supply heating for the device.

Additionally, to explore the impact of the enclosure thermal inertia on the inner temperature, it was essential to compare with the general radiative cooling experiment. Thus, the RCED with a 0.1 m × 0.1 m × 0.05 m space was set up (Fig. 2a and Fig. 3c). And the thickness of the side wall and the bottom were 0.1 m and 0.15 m, respectively. Compared with the slightly small inner space, the impact of the surroundings from the side wall and bottom was insignificant. Additionally, there existed two temperature points to measure the TRM and inner air, respectively.

The heat exchange coefficients of the TRM and sidewall were further investigated with the heat flow and temperature tester (CABR-RG09B), which were 2.5 W/(m^2·K) and 0.8 W/(m^2·K) respectively. The results indicated that the heat exchange coefficient of the TRM was about three times of the sidewall, raising the building load. The negative effects can be eliminated by radiative cooling in summer and offset by solar heating in winter.

The experimental devices were placed on the rooftop without any shelter and the calibrated K-type thermocouple (within ± 0.3 °C) was employed to measure the temperature variation during the experiment. Additionally, the temperature recorder was employed to collect the temperature of each measuring point and the digital high precision weather station was used to collect meteorological data, including dry bulb temperature, dew point temperature (within ± 0.3 °C), humidity (within ± 2%), wind speed (within ± 0.2 m/s) and solar irradiation (within ± 3%) with a collection time interval of 30 s (Fig. 3a).

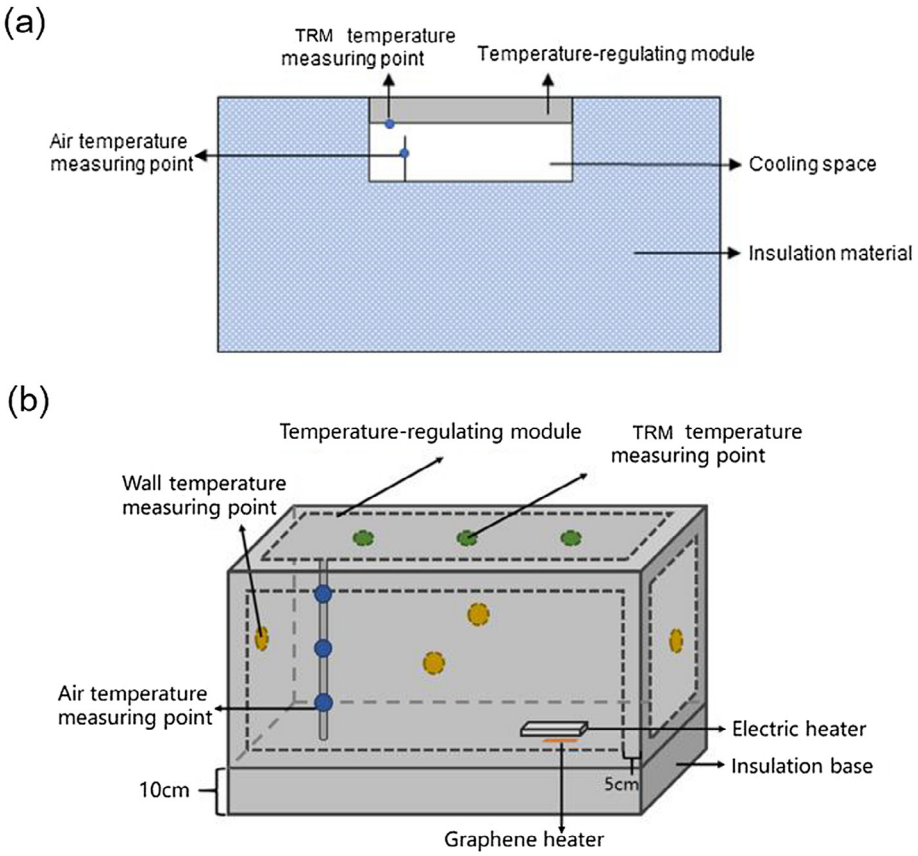

Fig. 2. Schematics of the experimental setup. (a) Schematic of the general radiative cooling experimental device (RCED). (b) Schematic of simulated building experimental device (SBED) with temperature measurement points and electric heater.

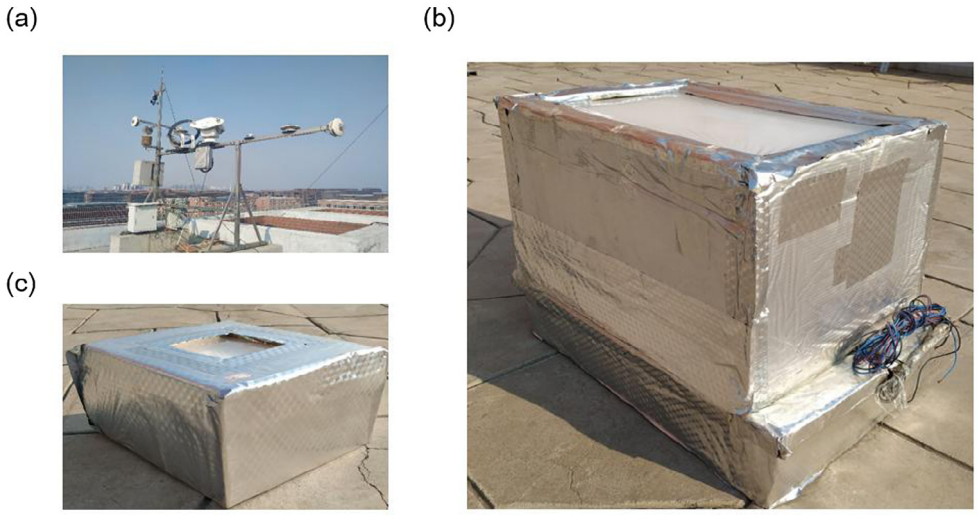

Fig. 3. Images of the experimental setup. (a) The digital high precision weather station. (b) Image of the simulated building experimental device (SBED). (c) Image of the general radiative cooling experimental device (RCED).

2.3. Spectral profile

The cooling materials (poly (vinylidene fluoride-co-hexafluoropropene) i.e. PVDF-HFP) was prepared by scalable phase inversion-based method, mainly employing the different evaporation rates of distilled water and acetone to induce the hierarchically porous structure of the cooling material. The solar reflectivity in 0.2–2.5μm was measured by UV–Vis-NIR spectrometer (UV3600plus, Japan) with a gold-plated integrating sphere, which is necessary for the short wavelength measurement. For the infrared measurement, the sample was adhered to a smooth aluminum substrate using alumina glue and Fourier transform infrared spectrometer (Bruker Hyperion 1000, Germany) was used to measure infrared spectral profiles of the sample [20]. The emissivity spectral profile was shown in Fig. 4.

3. Model analysis

To further explore the energy-saving potential of the proposed TRM in buildings, the transient model between the TRM and the building was developed systematically. And to evaluate the economy of the TRM in buildings, a simple economic analysis model was also employed in this work.

Table 1
The parameters of the single-storey residential building.

Region	Tianjin	Xi'an	Haikou	Las Vegas
Heat exchange coefficient of roof	0.35	0.45	0.8	0.32
Heat exchange coefficient of wall	0.43	0.7	1.75	0.42
Heat exchange coefficient of window	1.8	2.5	3	1.5
Window-wall ratio	0.275	0.275	0.312	0.2
Shading coefficient	0.6	0.6	0.45	0.6

3.1. Transient model

To capture the energy saving of the TRM in actual buildings, a single-storey residential building (240 m^2) was employ as the actual building model. The parameters are set as Table 1. Additionally, the summer cooling set temperature is 24 °C and the winter heating set temperature is 20 °C. To facilitate the establishment of the computational model, it is estimated that the internal disturbance load is about 3 W/m^2 from the power and operating time of human body, lighting and equipment.

The net cooling power of the TRM is affected by the instantaneous radiation intensity$P_{rad}(t)$, instantaneous solar absorption intensity $P_{sun}(t)$ and instantaneous non-radiative heat exchange intensity

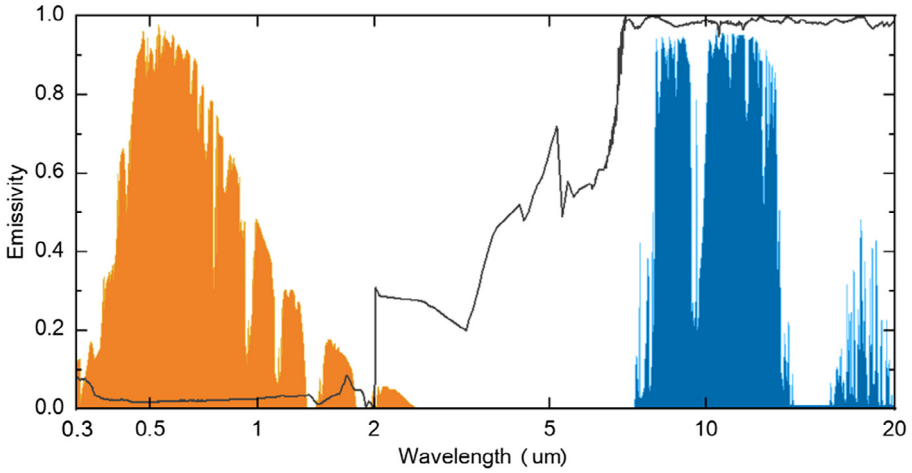

Fig. 4. The emissivity spectral profile of hierarchically porous cooling material in both solar and infrared bands. AM 1.5 solar spectral irradiance (orange) and atmosphere transmission distribution (blue) are given for reference.

$P_{cond+conv}(t)$. For the heating power of the TRM, only the instantaneous solar absorption intensity $P_{sun}(t)$ and instantaneous non-radiative heat exchange intensity $P_{cond+conv}(t)$ are considered. In the building model, the load $P_a(t)$ caused by temperature difference, the load $P_b(t)$ from solar radiation absorbed by enclosure, the load $P_c(t)$ caused by solar radiation entering the room through windows and the load $P_d(t)$ caused by human body, lighting and equipment are considered. The cooling capacity provided by the TRM is equal to the variation of the load in the building, thus the balance equations for summer and winter are given by equation (1) and (2) respectively [21].

$$c_v m\frac{dT}{dt} + P_a(t) + P_b(t) + P_c(t) + P_d(t) = P_{rad}(t) - P_{sun}(t) - P_{cond+conv}(t) \tag{1}$$

$$c_v m\frac{dT}{dt} + P_a(t) - P_b(t) - P_c(t) - P_d(t) = P_{sun}(t) - P_{cond+conv}(t) \tag{2}$$

where m is the air weight inside the building, c_v is the constant volume heat capacity, T is the inner air temperature and t is the calculating time.

The radiative intensity $P_{rad}(t)$ is the function of the TRM temperature T_r and the ambient dew point temperature $T_{dewpoint}$ [22].

$$P_{rad}(t) = f(T_r, T_{dewpoint}) \tag{3}$$

The solar absorption intensity $P_{sun}(t)$ is given by equation (4) [7].

$$P_{sun}(t) = \alpha_r I_{sun} A \tag{4}$$

where α_r is the solar absorption of cooling and heating mode, I_{sun} is the sunlight intensity, and A is the TRM area.

The non-radiative heat exchange intensity $P_{cond+conv}(t)$ was given by equation (5)-(7) [23].

$$P_{cond+conv}(t) = Ah_c(T_{amb} - T_r) \tag{5}$$

$$h_c = 2.8 + 3.0v \tag{6}$$

$$h_c = 8.3 + 2.5v \tag{7}$$

where T_{amb} is the ambient temperature, and h_c is the non-radiative heat exchange coefficient [24]. According to whether there exists a cover shield on the outer surface of the TRM, the h_c is given by equation (6) [21] in summer and equation (7) in winter [15], where v is the wind speed.

The load caused by temperature difference $P_a(t)$ is given by equation (8)

$$P_a(t) = \sum U_i A_i (T_{amb} - T) \tag{8}$$

where U_i is heat exchange coefficient of wall, window and roof respectively, and A_i is area of wall, window and roof respectively.

The load from sunlight absorbed by enclosure $P_b(t)$ is given by equation (9).

$$P_b(t) = \sum \alpha_l A_l I_l \tag{9}$$

where α_l is the solar absorptivity of each side of the enclosure, A_l is the area of each side of the enclosure, and I_l is the incident intensity of solar radiation on each side of the enclosure.

The load caused by solar radiation entering the room through windows $P_c(t)$ is given by equation (10)

$$P_c(t) = \sum \tau A_t I_t \tag{10}$$

where τ is the solar transmissivity of the window, A_t is the area of each window, and I_t is the incident intensity of solar radiation for each window.

The load caused by human body, lighting and equipment $P_d(t)$ is given by equation (11)

$$P_d(t) = WA_0 \tag{11}$$

where W is the load from human body, lighting and equipment per unit area, and A_0 is the building area.

3.2. Economic analysis model

In the scenario that the TRM and the split air conditioner jointly provides cooling/heating for the building, the optimal TRM area with the lowest cost as the goal can be achieved. The simple payback period SPP was given by equation (12) [25].

$$SPP = \frac{C_R + C_A - C_S}{(E_{S1} - E_{A1} + E_{S2} - E_{A2})P_E} \tag{12}$$

where C_R is the cost of the building employing the TRM, C_A is the cost of the air conditioning system after employing the TRM, and the split air conditioning [26] was 404.5 \$/kW. C_S is the cost of air conditioning alone, E_{S1} and E_{S2} are the summer and winter electricity consumption of the split air conditioning, respectively, and E_{A1} and E_{A2} are the summer and winter electricity consumption by employing the TRM and the split air conditioning respectively, and P_E is the electricity price, which is 0.12 \$/kWh in this paper [25].

In addition, the maximum acceptable incremental cost AIC_{max} proposed by Fernandez et al. [27] is employed to evaluate the economy of the TRM, as shown in equation (13).

$$AIC_{max} = \frac{(E_{S1} - E_{A1} + E_{S2} - E_{A2})P_E SPP}{A} \tag{13}$$

where A is the TRM area.

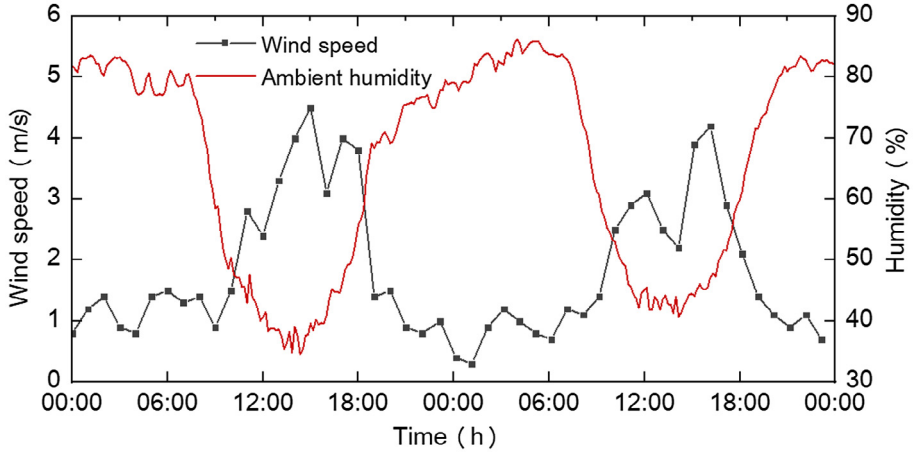

Fig. 5. Variations of wind speed and humidity during the experiment from February 14 to February 15.

4. Results

In this section, radiative cooling and solar heating performance of the TRM are presented in the cooling and heating experiments. Subsequently, energy saving potential of the TRM in different areas is discussed to demonstrate the superiority of direct combination of radiative cooling technology and buildings.

4.1. Radiative cooling performance

From February 14 to February 15, 2019, the summer cooling experiments were conducted on a three-storey rooftop (8.2 m above sea level) in Sanya (18°45′N, 109°10′W) with high temperature and humidity climate. Over the consecutive two days experiment, there existed some scattered clouds in the morning, slightly reducing the cooling performance, whereas it was clear and cloudless at other time. In the daytime, the wind speed was slightly high, with the maximum of 4 m/s, and the humidity was fairly low, with the minimum of about 40%, while at night, the results were just the opposite (Fig. 5).

Fig. 6 depicted the temperature variations of each measuring point in the SBED on February 15. The temperature of the TRM, sidewall and inner air varied with the ambient temperature and were all lower than the ambient. And the TRM temperature was slightly lower than the sidewall and inner air temperature, indicating that the TRM provided cooling capacity for the experimental device interior. When the solar irradiation reached 750 W/m^2 and the maximum ambient temperature reached 34 °C, the inner air temperature was only 27.5 °C. With a summer cooling setting temperature of 24 °C (dashed line in Fig. 6), the air conditioning was only on from 11:30 am to 6 pm every day to provide partial cooling. Note that the nighttime indoor air temperature during the experiment reduced to about 15 °C, which seriously affected the indoor comfort. With the energy storage system to store the excess cooling capacity at night and supply the indoor in the daytime, it will further cut down the opening time of air conditioning and reduce the energy consumption, demonstrating the great energy-saving potential in direct way.

The actual building envelope had a certain thermal inertia, that is, the variation of the ambient will have a certain delay and attenuation for the indoor air, beneficial to the indoor temperature control. Note that the previous radiative cooling experiments ignored the impact of the ambient on the device interior through the sidewalls and can't capture the actual performance of the building employing the TRM. Therefore, the inner temperature variation of the SBED, SBCD and RCED were investigated to explore the impact of thermal mass on February 14–15 (Fig. 7). The air temperature in the SBCD was higher than 24 °C for most of the day and the maximum could reached 34 °C (red curve in Fig. 7), indicating that abundant cooling capacity from the air conditioning system was essential to meet the cooling load. Additionally, compared to the RCED (blue curve in Fig. 7), the air temperature variation in the SBED (orange curve in Fig. 7) was significantly delayed. More specifically, the air temperature of the SBED in the morning was slightly lower than that in the RCED, while that in the afternoon was slightly higher. Recognizing that the wall insulation employed in the experimental device was silghtly thin, the corresponding attenuation was not observed. In principle, the thermal inertia of the enclosure can slow down the indoor temperature drop at night, weakening the negative impact in direct way to some extent.

4.2. Solar heating performance

To probe the actual operation effect of the TRM in winter, the winter experiments were conducted on a rooftop (about 9.5 m above sea level) in Tianjin (39°05′N, 117°10′ E), from March 1 to March 3, 2019. There was less cloudiness on March 3 and it was more clear and cloudless during the first two days. Similar to the summer experiments, the daytime wind speed was low and the humidity was high, while the nighttime wind speed was high and the humidity was low (Fig. 8).

The winter experiment of the SBED without additional heating supply was carried out on March 1. When the TRM was in the cooling mode (Fig. 9), the winter experimental results were similar to the corresponding summer experiments. The temperature of the TRM, sidewall and inner air were all lower than the ambient. Yet, due to the significantly low ambient temperature in winter (with the maximum of about 18 °C), the TRM in cooling mode led to the dramatically lower indoor temperature (even lower than 0 °C at night), i.e. negative impact of radiative cooling in winter. The negative impact not only seriously had a significant impact on the indoor comfort, but also increased the heating energy consumption.

To address the negative impact of the radiative cooling technology, the proposed TRM can turn to heating mode. The TRM heating experiment was plotted in Fig. 10. It can be clearly seen that in the daytime the temperature of TRM, wall and air were all substantially improved. The TRM temperature even reached 32 °C in the daytime, when the solar radiation reached about 450 W/m^2, while the indoor temperature was only 25 °C due to abundant heat dissipation. Additionally, It was noteworthy that the nighttime temperature was slightly lower than the ambient, with the minimum value closing to 0 °C. The main reason behind was that the solar absorbing material had slight mid-infrared emissivity, further reducing the TRM temperature. With a winter heating setting temperature of 20 °C (dashed line in Fig. 10), there was about a quarter of the day without the need of additional heating during the experiment.

To further explore the actual performance of the TRM with additional heating supply in the winter of mid-latitudes, the electric heater was employed to provide heating for the experimental devices from about 6:30 pm on March 2 (the vertical dashed line in Fig. 11) to mimic building heating supply with a setting temperature of 20 °C. When the inner temperature was higher than the setting temperature, the heater stopped heating, otherwise started heating. It can be clearly seen from Fig. 11 that the inner air temperature was substantially improved at night. Owing to the high heat exchange coefficient of the TRM, the nighttime indoor temperature was lower than the setting temperature and the minimum temperature reached 15 °C, which gave rise to the increase of heating load. Additionally, even in the daytime with high clouds (fluctuating grey curve in Fig. 11), the inner air temperature was closed to the heating experiment on March 1(Fig. 10) and there still existed more than a quarter of the day without the heating need. To further improve the energy saving, it was the appealing candidate to store the excess heat in the daytime to offset the nighttime heating load.

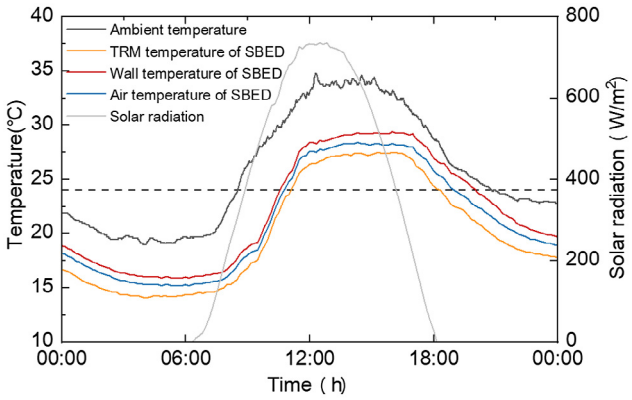

Fig. 6. The temperature variations with time in the SBED on February 15, including ambient temperature (black curve), TRM temperature (orange curve), wall temperature (red curve) and air temperature (blue curve). Solar radiation intensity (grey curve) is given for reference.

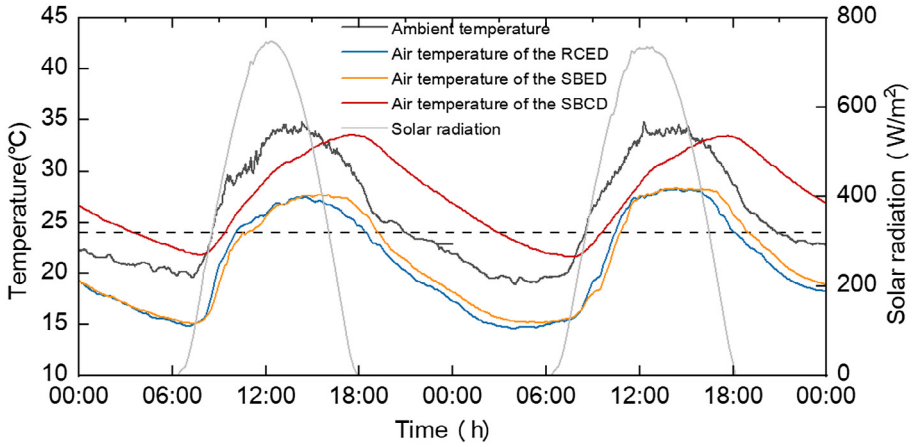

Fig. 7. The inner air temperature variations of the SBED (orange curve), SBCD (red curve) and RCED (blue curve) from February 14 to February 15. Solar radiation intensity (grey curve) is given for reference.

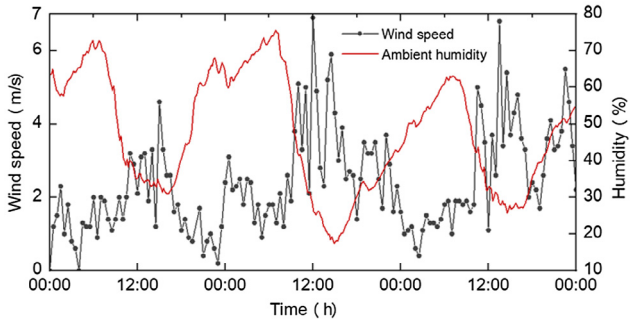

Fig. 8. Variations of wind speed and humidity during the winter experiment from March 1 to March 3.

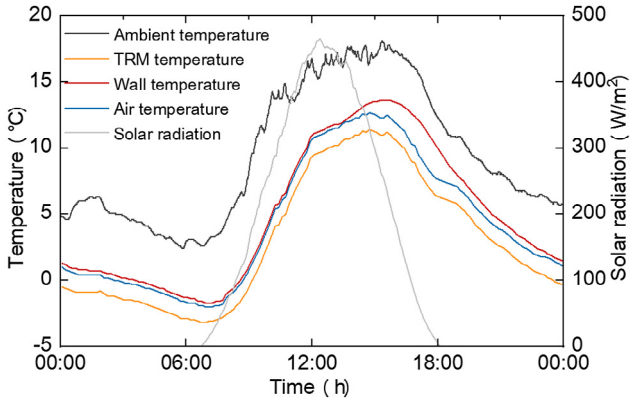

Fig. 9. The temperature variations of the SBED in cooling mode on March 1, including ambient temperature (black curve), TRM temperature (orange curve), wall temperature (red curve) and air temperature (blue curve). Solar radiation intensity (grey curve) is given for reference.

4.3. Model validation

To explore the energy saving of the TRM in different areas, MATLAB software was employed the to establish computational model in summer and winter under different climates. The summer and winter computational models were validated by the whole experimental results on February 14–15 and March 1–3, respectively. The modeling temperature in the experimental device could be captured by inputting meteorological parameters during the experiment.

The relative error of the measured and modeling results in summer was within 5% (Fig. 12a). Specifically, the modeling temperature at night was in good agreement with the measured, while the great differences occurred in the daytime, mainly due to a certain thermal inertia of the device, which delayed the variation of indoor temperature. However, it had weak impact on the total energy consumption throughout the day. In winter, the modeling and measured results showed nearly no difference before the additional heating supply. The main reason behind was that the thermal inertia had less impact, due to the high wind speed in winter and no cover shield outside the TRM. However, after the additional heating supply (vertical dashed line in Fig. 12b), the difference between the measured and modeling temperature was slightly large, but the whole relative error was still less than 5%.

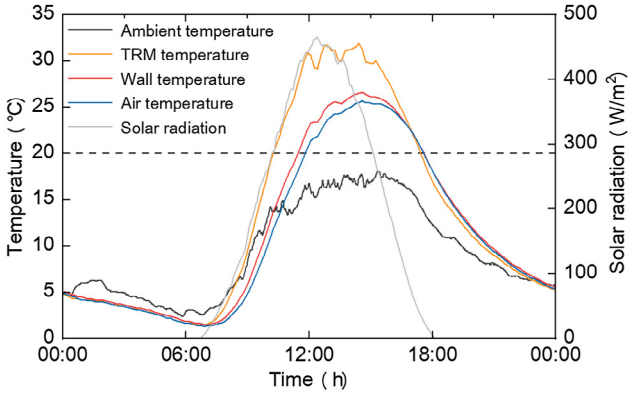

Fig. 10. The temperature variations of the SBED in heating mode on March 1, including ambient temperature (black curve), TRM temperature (orange curve), wall temperature (red curve) and air temperature (blue curve). Solar radiation intensity (grey curve) is given for reference.

4.4. Energy saving

The direct combination of radiative cooling and buildings holds the promising potential to address the problem of high energy consumption in buildings, including single-storey buildings (single-storey residential buildings and factories, etc.) and space-connected buildings (shopping malls, stations, airports and the atriums of commercial office building, etc.). A single-storey residential building with an area of 240 m^2 was employed as the example to demonstrate the great potential of the direct way. Additionally, Energy plus software was used to capture the cooling and heating load in Typical Meteorological Year. And the single-storey residential buildings employed split air conditionings, which had low energy efficiency (about 3 in summer and 2.75 in winter

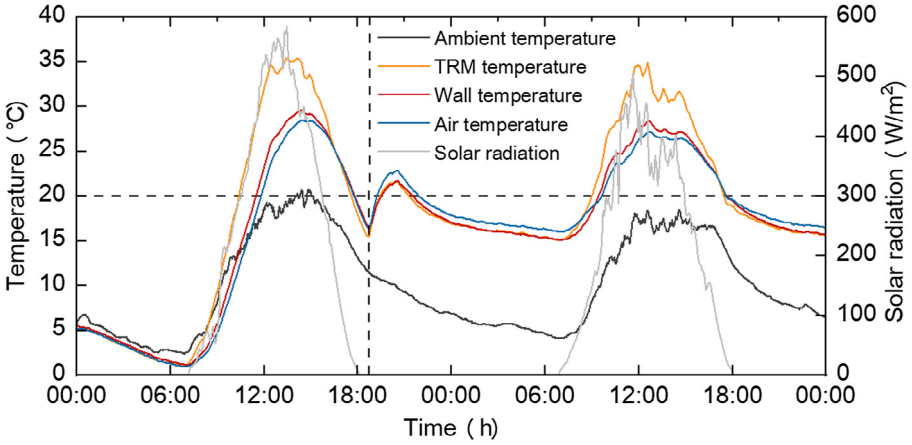

Fig. 11. The temperature variations of the SBED in heating mode from March 2 to March 3, including ambient temperature (black curve), TRM temperature (orange curve), wall temperature (red curve) and air temperature (blue curve). Solar radiation intensity (grey curve) is given for reference (heating supply started from about 6:30 pm on March 2).

[28]). With the 60% roof area employing the TRM, cooling/heating capacity provided by the module was calculated with the model in cooling season (from May 1 to August 31) and heating season (from November 15 to March 15). When the TRM can't meet the indoor cooling/heating demand, the air conditioning system provided the rest energy (Fig. 13).

4.4.1. Energy saving potential in cooling season

It can be clearly seen from Fig. 14 that indoor cooling loads at the beginning and end of the cooling season were fairly low, while the cooling capacity provided by the TRM was significantly higher. However, it was reverse in the mid cooling season, mainly due to more rainy days in Tianjin. Thus, radiative cooling power was extremely low, even was negative sometimes, meanwhile the heat exchange coefficient of the TRM was fairly large, increasing the indoor cooling load (Fig. 14a and b).

When considering the energy saving in direct way, it was essential to correct the building cooling load when the cooling capacity provided

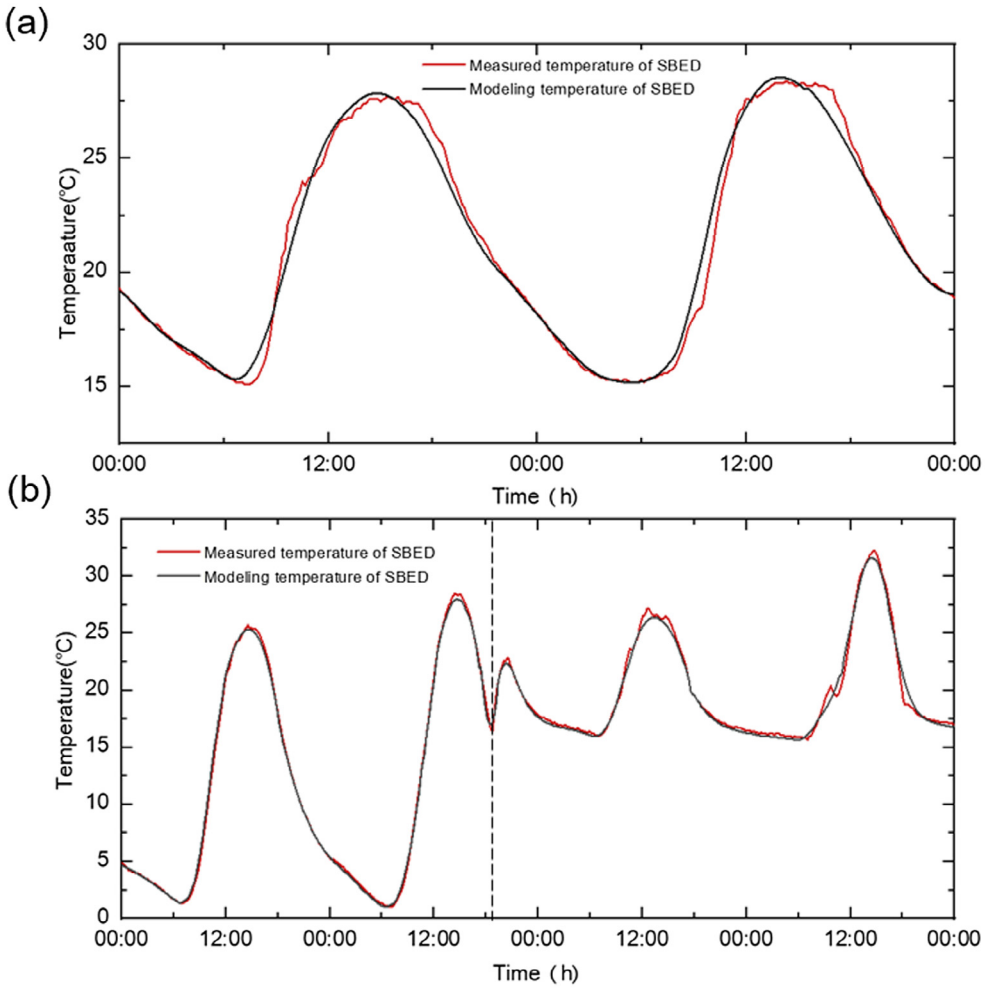

Fig. 12. Model validation in summer and winter. (a) Measured and modeling air temperature of SBED in summer. (b) Measured and modeling air temperature of SBED in winter.

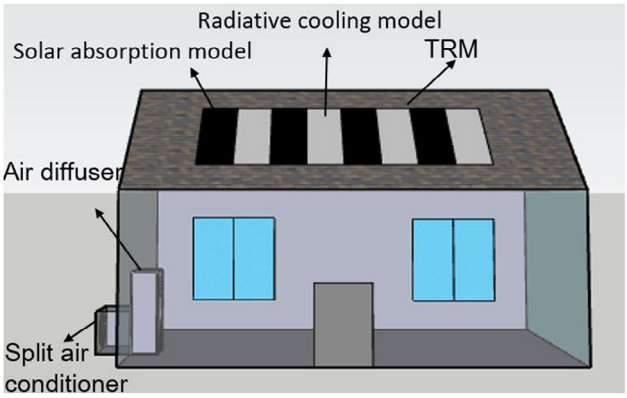

Fig. 13. Schematic of the single-storey residential building employing the TRM and the air conditioning system.

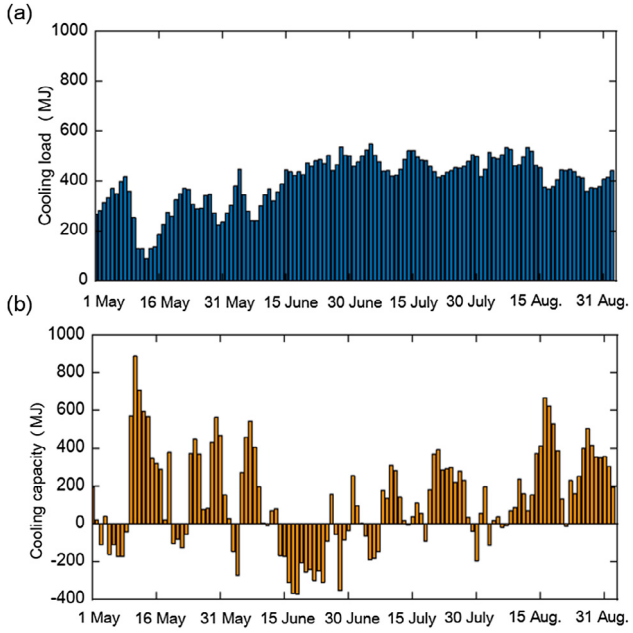

Fig. 14. The energy variations of the building with the TRM in cooling season. (a) Cooling load of the building. (b) Cooling capacity provided by the TRM.

by the TRM was negative. Additionally, when the cooling capacity was higher than the cooling load, the cooling capacity should be corrected (Excessive cooling capacity was invalid). The daily energy saving was plotted in Fig. 15, wherein the value of energy saving greater than three was taken as three, indicating the excess cooling capacity. The whole summer energy saving of the building employing the TRM was about 42.4%, and the corresponding electricity saving was 963.5 kWh. With the energy storage system to compensate for the time asynchrony between cooling load and cooling capacity [29], the energy saving in summer can theoretically reach 63.7%, and the corresponding electricity saving was 1449.1 kWh.

The energy saving of different TRM areas in different regions, including two coastal cities, Tianjin and Haikou (20°1′N,110°19′E), two inland cities, Xi'an (34°16′N 108°54′E) and Las Vegas, was further probed. The cooling season in Tianjin, Xi'an and Las Vegas was from May 1 to August 31, while that for Haikou were all year round. The energy saving in direct cooling and with energy storage system in different regions both increased with the TRM area (Fig. 16a and b). Note that the energy saving of direct cooling in Tianjin and Haikou reached a peak with the 60% and 50% roof area, respectively, while that in Las Vegas and Xi'an had the peak with the 90% roof area, mainly due to the meteorological parameters of different locations. However, there existed no such peak for the energy saving with energy storage system. It should be noted that the energy saving of direct cooling with the 60% roof area employing the TRM in Las Vegas reached 29.7%, which was substantially higher than the indirect way. Typically, with a 20% roof area employing the TRM, it can achieve the same energy saving as the indirect way [8], demonstrating the promising potential of the direct combination of radiative cooling technology and buildings.

4.4.2. *Energy saving potential in heating season*

Subsequently, the energy saving of the residential buildings with the 60% roof area employing the TRM in winter was investigated. Similarly, the heating load of the building and heating capacity supplied by the TRM in winter were not synchronized in time. Specifically, there existed abundant days with negative heating capacity, mainly distributing in the early heating season, while at the end of the heating season, the TRM provided excess heating capacity for the building (Fig. 17a and b). The corresponding daily energy saving was plotted in Fig. 18. Note that the solar heating was limited by day and night. Although the TRM absorbed abundant solar energy during the daytime, the energy can't still meet the abundant heating demand at night. Energy storage system can be employed to address the problem that the heating supplied by the TRM was not synchronized with the heating demand. Therefore, the theoretical energy saving with the energy storage system in winter was discussed here, and it can reach 14.7%, with

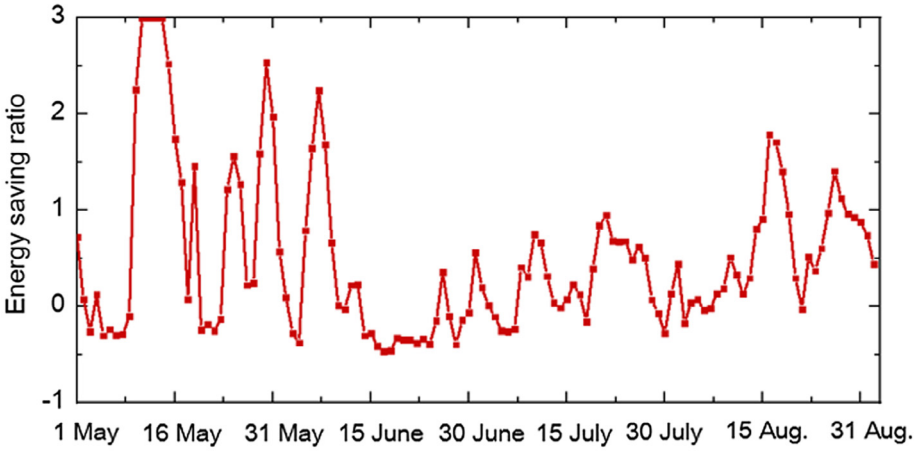

Fig. 15. The daily energy saving of the building with the TRM in cooling season.

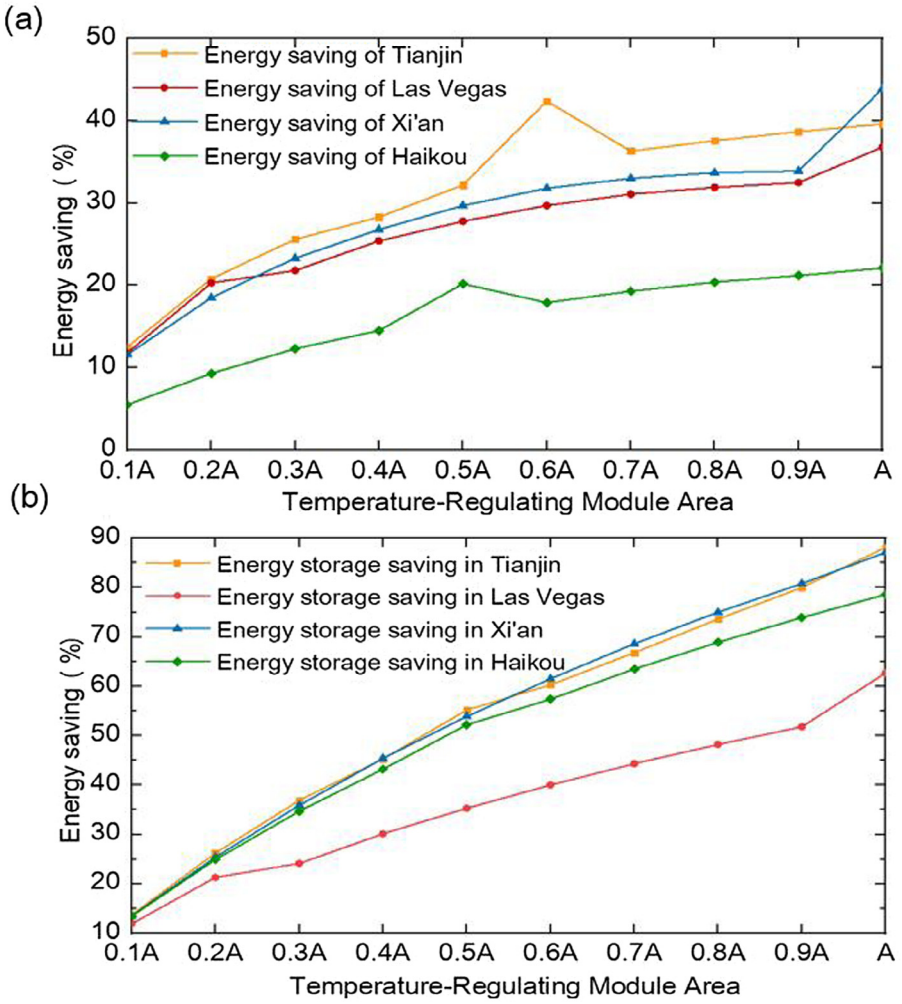

Fig. 16. Energy saving of the building employing the TRM in different areas. (a) Variations of direct energy saving with the TRM area. (b) Variations of energy storage saving with the TRM area. Abscissa axis *A* is the roof area.

the corresponding electricity saving of 492 kWh.

5. Discussion

There are some practical problems in direct way, including the conversion of cooling and heating mode, leak problem, the combination of TRM and energy storage system and economy. These challenges were further discussed and the corresponding feasible solutions were proposed in this Section.

With respect to the conversion methods, a simple but viable design was provided, employing a rotating shaft to control the conversion of cooling and heating mode of the TRM with setting size (Fig. 19). Additionally, the number of cooling and heating mode can be determined according to the actual cooling and heating demand, so as to maximize indoor comfort. However, it was essential to handle the gap between the TRMs to avoid leakage and penetration. Therefore, a double-layer structure including the TRM and the wind shield with high infrared and solar transmittance was proposed in Fig. 19 (blue film). And the structure can not only reduce convection heat loss in cooling/heating mode, but also improve the overall airtightness of buildings with the TRM.

As discussed, employing energy storage system to store the excess cooling/heating capacity greatly improved the energy saving of the TRM. Further investigations revealed that the energy storage system can also address the surface condensation of the TRM, which was owing to excess cooling capacity. A feasible design that integrated the TRM with the coil was provided to conduct the combination of the TRM and energy storage system (Fig. 20a and b). The coil between the porous cooling material and the solar absorbing material can turn around the axis with the TRM. Fig. 20c depicted the schematic of the building employing the TRM with energy storage system. When there was excessive cooling/heating capacity, turn on the pump to start energy storage, otherwise close the pump and the TRM provide cooling/heating capacity for buildings alone. When the cooling/heating capacity provided by the TRM was insufficient to meet indoor demand, turn on the pump to release the cooling/heating capacity in the energy storage device. If it was still insufficient, turn on the air conditioning system. The ingenious design can minimize the running time of air conditioning system and maximize energy saving in buildings employing the TRM.

The energy saving of the building employing the TRM with different areas was subsequently discussed, but note that it was meaningless to optimize the TRM area without considering the cost. With 8 years as an acceptable payback period [25], the optimum area of the TRM was determined when both the TRM and the split air conditioning jointly provided cooling/heating capacity for the indoor. The optimal area of the TRM in Tianjin was 62 m^2 with an energy saving of 24% in summer, while that in Xi'an was 52 m^2 with an energy saving of 19.5% in summer. It was estimated that the cost of the TRM was about 50 $\$/m^2$ according to the price of cooling material, the solar absorbing material, aluminum conductor and the polyethylene film (The cost will reduce with mass production). Taking five years as the acceptable payback

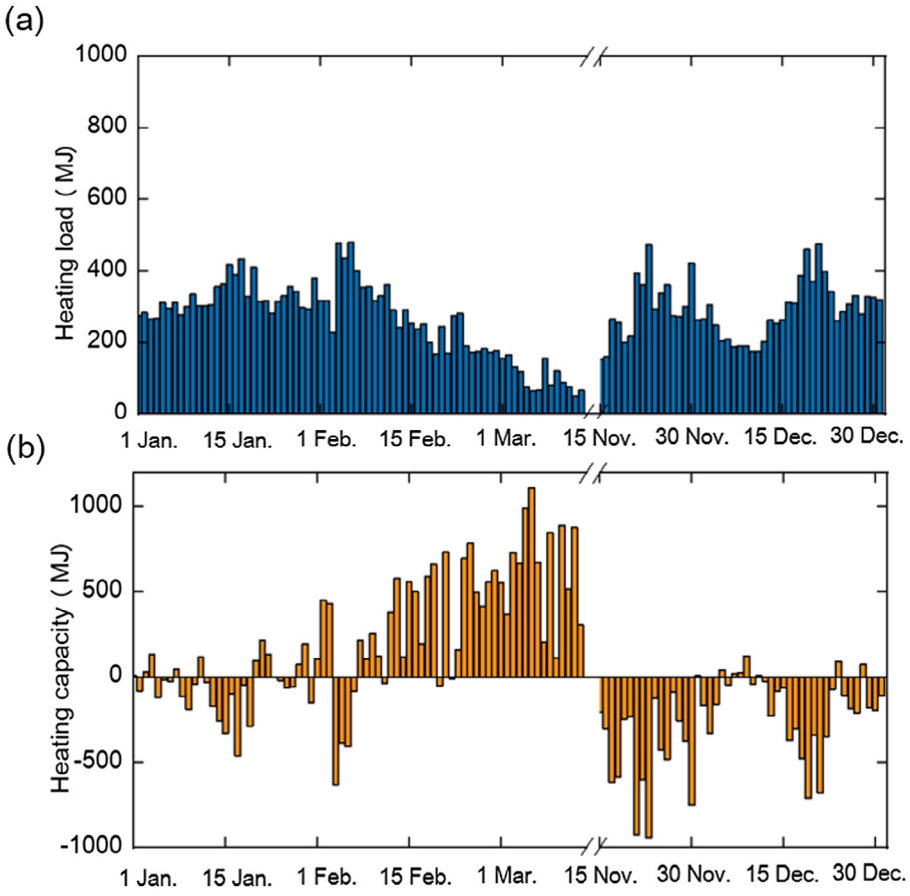

Fig. 17. The energy variations of the building with the TRM in heating season. (a) Heating load of the building. (b) Heating capacity provided by the TRM.

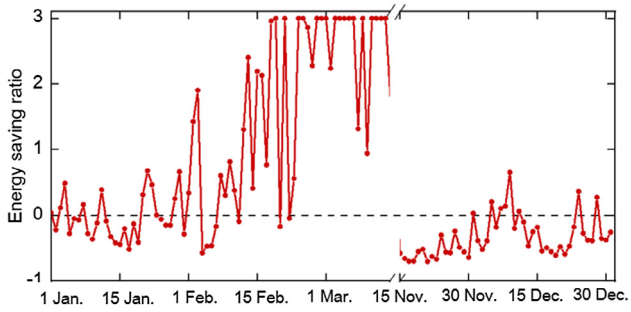

Fig. 18. The daily energy saving of the building with the TRM in heating season.

period, the maximum acceptable incremental cost for Tianjin and Xi'an were 16.4 $/m^2 and 14.3 $/m^2, respectively, while the acceptable cost increment cost reported by Fernandez et al. [27] was only 2.5–6.25 $/m^2. With an acceptable payback period of 8 years, the maximum acceptable incremental cost in Tianjin and Xi'an reached 26.2 $/m^2 and 22.9 $/m^2, respectively.

6. Conclusion

In view of lack of work on direct combination of daytime radiative cooling and buildings and the negative impact of the direct way, a temperature-regulating module based on the combination of radiative cooling and solar heating was proposed and the radiative cooling and solar heating experiments were conduct to explore the performance of

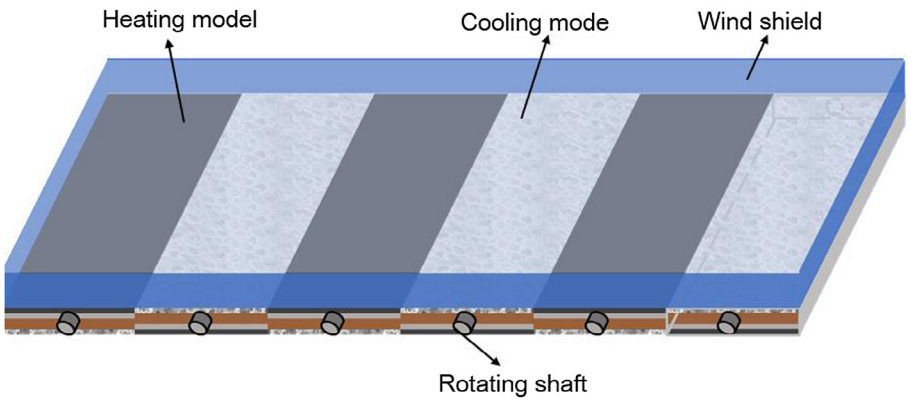

Fig. 19. Schematics of a viable design to control the conversion of cooling and heating mode of the TRM.

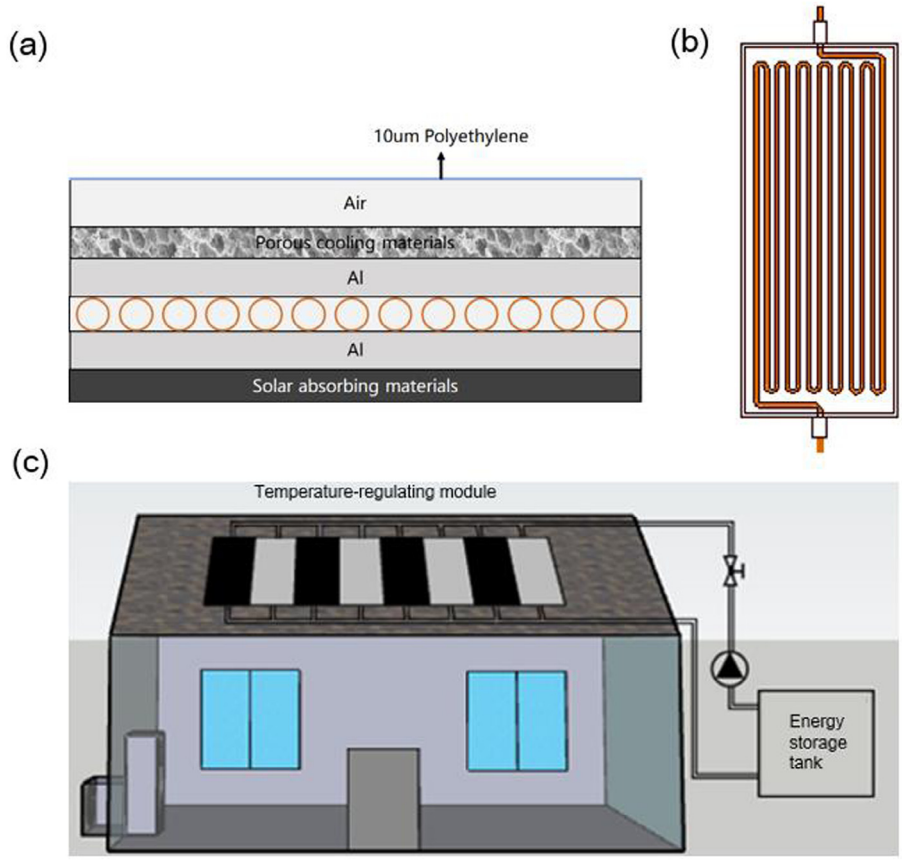

Fig. 20. Combination of the TRM and energy storage system. (a) Cross-section of the TRM with the coil. (a) Schematic of the combination of the TRM and the coil. (c) Schematic of the building employing the TRM with energy storage system.

the TRM in summer and winter. The work drew the following conclusions:

(1) In summer experiments, the maximum indoor temperature was only 27.5 ˚C with the ambient temperature of 34 ˚C in low latitude areas and the air conditioning system was on for only about a quarter of the day.
(2) In winter experiments, the indoor temperature can reach 25 ˚C in the daytime without additional heat supply and about a quarter of the day didn't require heating in winter.
(3) The modeling results revealed that the electricity saving of 42.4% (963.5 kWh) can be achieved in summer, while that was 63.7% (1449.1 kWh) when coupling with energy storage system. And, the cooling area in direct way was only one third of that in indirect way (in Las Vegas).
(4) With an acceptable payback period of 8 years, the maximum acceptable incremental cost was 26.2 $/m^2.

Author contribution

J.L., D.Z. and S.J. executed the experiments. D.Z., S.J. and Z.Z. performed the modeling. J.L.F.G. J.Z. and Z.Z. edited and reviewed the manuscript. All authors contributed to the work. Z.Z. and J.L. are co-corresponding author.

Declaration of Competing Interest

The authors declare that they have no known competing financial interests or personal relationships that could have appeared to influence the work reported in this paper.

Acknowledgements

This work was supported by the Tianjin science and technology commission of China (Contract nos. 18ZXAQSF00030). The authors acknowledge them for their support and assistance in this study.

References

[1] Lake A, Rezaie B, Beyerlein S. Review of district heating and cooling systems for a sustainable future. Renew Sustain Energy Rev 2017;67:417–25.
[2] Chua KJ, Chou SK, Yang WM, Yan J. Achieving better energy-efficient air conditioning – a review of technologies and strategies. Appl Energy 2013;104:87–104.
[3] Chen Z, Zhu L, Raman A, Fan S. Radiative cooling to deep sub-freezing temperatures through a 24-h day-night cycle. Nat Commun 2016;7:13729.
[4] Gentle AR, Smith GB. Radiative heat pumping from the Earth using surface phonon resonant nanoparticles. Nano Lett 2010;10:373–9.
[5] Zhao B, Hu M, Ao X, Chen N, Pei G. Radiative cooling: a review of fundamentals, materials, applications, and prospects. Appl Energy 2019;236:489–513.
[6] Li N, Wang J, Liu D, Huang X, Xu Z, Zhang C, et al. Selective spectral optical properties and structure of aluminum phosphate for daytime passive radiative cooling application. Sol Energy Mater Sol Cells 2019;194:103–10.
[7] Hossain MM, Gu M. Radiative cooling: principles, progress, and potentials. Adv Sci 2016;3:1500360.
[8] Raman AP, Anoma MA, Zhu L, Rephaeli E, Fan S. Passive radiative cooling below ambient air temperature under direct sunlight. Nature 2014;515:540–4.
[9] Gentle AR, Smith GB. A subambient open roof surface under the mid-summer sun. Adv Sci 2015;2:1500119.
[10] Kou J, Jurado Z, Chen Z, Fan S, Minnich AJ. Daytime radiative cooling using near-black infrared emitters. ACS Photonics 2017;4:626–30.
[11] Zhai Y, Ma Y, David SN, Zhao D, Lou R, Tan G, et al. Scalable-manufactured randomized glass-polymer hybrid metamaterial for daytime radiative cooling. Science 2017;355:1062–6.
[12] Atiganyanun S, Plumley JB, Han SJ, Hsu K, Cytrynbaum J, Peng TL, et al. Effective radiative cooling by paint-format microsphere-based photonic random media. ACS Photonics 2018;5:1181–7.
[13] Mandal J, Fu Y, Overvig A, Jia M, Sun K, Shi N, et al. Hierarchically porous polymer coatings for highly efficient passive daytime radiative cooling. Science 2018;362:315–9.

[14] Goldstein EA, Raman AP, Fan S. Sub-ambient non-evaporative fluid cooling with the sky. Nat Energy 2017;2:17143.
[15] Zhao D, Aili A, Zhai Y, Lu J, Kidd D, Tan G, et al. Subambient cooling of water: toward real-world applications of daytime radiative cooling. Joule 2019;3:111–23.
[16] Aili A, Zhao D, Lu J, Zhai Y, Yin X, Tan G, et al. A kW-scale, 24-hour continuously operational, radiative sky cooling system: experimental demonstration and predictive modeling. Energy Convers Manage 2019;186:586–96.
[17] Liu J, Zhou Z, Zhang J, Feng W, Zuo J. Advances and challenges in commercializing radiative cooling. Mater Today Phys 2019:100161.
[18] Ono M, Chen K, Li W, Fan S. Self-adaptive radiative cooling based on phase change materials. Opt Express 2018;26:A777–87.
[19] Fan D, Li Q, Xuan Y, Tan H, Fang J. Temperature-dependent infrared properties of Ca doped (La, Sr)MnO3 compositions with potential thermal control application. Appl Therm Eng 2013;51:255–61.
[20] Fu Y, Yang J, Su YS, Du W, Ma YG. Daytime passive radiative cooler using porous alumina. Sol Energy Mater Sol Cells 2019;191:50–4.
[21] Zeyghami M, Goswami DY, Stefanakos E. A review of clear sky radiative cooling developments and applications in renewable power systems and passive building cooling. Sol Energy Mater Sol Cells 2018;178:115–28.
[22] Fan D, Sun H, Li Q. Thermal control properties of radiative cooling foil based on transparent fluorinated polyimide. Sol Energy Mater Sol Cells 2019;195:250–7.
[23] Ao X, Hu M, Zhao B, Chen N, Pei G, Zou C. Preliminary experimental study of a specular and a diffuse surface for daytime radiative cooling. Sol Energy Mater Sol Cells 2019;191:290–6.
[24] Aili A, Wei Z, Chen Y, Zhao D, Yang R, Yin X. Selection of polymers with functional groups for day-time radiative cooling. Mater Today Phys 2019;10:100127.
[25] Zhang K, Zhao D, Yin X, Yang R, Tan G. Energy saving and economic analysis of a new hybrid radiative cooling system for single-family houses in the USA. Appl Energy 2018;224:371–81.
[26] Xiong J, Yao R, Grimmond S, Zhang Q, Li B. A hierarchical climatic zoning method for energy efficient building design applied in the region with diverse climate characteristics. Energy Build 2019;186:355–67.
[27] Fernandez N, Wang W, Alvine KJ, Katipamula S. Energy savings potential of radiative cooling technologies. Pacific Northwest National Laboratory (PNNL), Richland, WA (US); 2015 < https://www.osti.gov/ scitech/biblio/1234791 > .
[28] Long J, Zhang R, Lu J, Xu F. Heat transfer performance of an integrated solar-air source heat pump evaporator. Energy Convers Manage 2019;184:626–35.
[29] Zhou Z, Liu J, Wang C, Huang X, Gao F, Zhang S, et al. Research on the application of phase-change heat storage in centralized solar hot water system. J Clean Prod 2018;198:1262–75.